Recent developments in type-II superlattice detectors at IRnova AB

Hedda Malm[1, *], Rickard Marcks von Würtemberg[1], Carl Asplund[1], Henk Martijn[1], Amir Karim[2], Oscar Gustafsson[3], Elena Plis[4], Sanjay Krishna[4]
[1] IRnova AB, Electrum 236, SE-164 40 Kista, Sweden
[2] Acreo AB, Electrum 236, SE-164 40 Kista, Sweden
[3] School of Information and Communication Technology, Royal Institute of Technology, Sweden
[4] Center for High Technology Materials, University of New Mexico, Albuquerque, USA

ABSTRACT

A mid wave infrared type-II superlattice focal plane array with 320x256 pixels, 30 µm pitch and 90 % fill factor was fabricated in house, using a conventional homojunction p-i-n photodiode design and the ISC9705 readout circuit. High-quality imaging up to 110 K is demonstrated with the substrate fully removed. The absorber is 2 µm thick, and no anti-reflection coating was used, so there is still room for significant improvement of the quantum efficiency, which is in the 40 % range.
Studies of the dark current vs. temperature behavior indicate that the device is limited by Shockley-Read-Hall generation from the depletion region. The activation energy of this dark current component is 0.13 eV, suggesting an unidentified recombination center positioned halfway into the 0.24 eV bandgap.
Furthermore, we report on detectors with 100 % cut-off at 13 µm. The dark current density at 60 K and -50 mV bias is $2x10^{-4}$ A/cm^2. Quantum efficiency, NETD and BLIP temperature are also calculated.
Position-sensitive photocurrent measurements on mesa-etched superlattice material were made at low temperatures using a focused laser spot. The lateral diffusion length for holes was extracted and is reported.

Keywords: type II superlattice, MWIR, VLWIR, photodetector, InAs/GaSb, T2SL, dark current, diffusion length

1. INTRODUCTION

Large imaging infrared detectors covering the wavelength range 3-15 µm are of high interest for several industrial, as well as surveillance and earth observation applications. Recently, type-II InAs/GaSb based strained layer superlattice (T2SL) structures have emerged as a promising material for high-performance infrared photodetection for mid wave (MWIR, 3-5 µm) and long wave IR (LWIR, 8-12 µm and VLWIR, 11-15 µm). Currently, high end IR detection systems are predominantly based on mercury cadmium telluride (MCT), indium antimonide (InSb), and quantum well infrared photodetector (QWIP) technologies. However, several interesting properties of the type-II superlattice material offer a possible alternative to the current technologies [1]. T2SL benefits from a larger carrier effective mass, compared to the state-of-the-art MCT technology, leading to reduced tunnelling currents [2, 3] and significant reduction of Auger recombination rate [4]. However, this remains a theoretical advantage, since present state of the art T2SL detectors for MWIR application are depletion-current limited below approximately 140 K and only diffusion current limited at temperatures above that. The generation process is Shockley-Read-Hall, *i.e.* generation via deep defects in the bandgap. Lifetime is typically of the order of a few 10 ns, that is two orders of magnitude shorter than for the Auger-limited MCT [5].

InAs/GaSb strained layer superlattice is a III-V material with a number of advantages that include the possibility to perform low cost volume production and can lead to good uniformity. In contrast to QWIPs, these detectors operate at normal incidence and no grating is needed. Surface leakage currents on mesa sidewalls are a problem especially for the performance of LWIR and VLWIR detectors, but also for detectors in the MWIR range. This problem needs to be carefully addressed by employing smart design and/or surface passivation coatings. Nevertheless, recent results indicate that T2SL FPA performance is approaching MCT, both in the MWIR [6] and the LWIR [7] bands.

* Corresponding author: hedda.malm@ir-nova.se, +46 (0)8 793 66 14

Infrared Technology and Applications XXXVIII, edited by Bjørn F. Andresen, Gabor F. Fulop, Paul R. Norton,
Proc. of SPIE Vol. 8353, 83530T · © 2012 SPIE · CCC code: 0277-786X/12/$18 · doi: 10.1117/12.918992

As the T2SL material quality is getting better, the chance to compete with present technologies increases. Dual-band MWIR/MWIR back-to-back photodiode FPA modules are currently in series production. While representing a formidable technical task in many ways, this special application does however not require high operating temperature [8]. For T2SL to compete with present technologies, pixels need to be smaller and the number of pixels larger. To investigate these possibilities, the detector's dark current behaviour was studied in order to understand the parameters that need to be optimized.

P-on-n superlattice detectors preferably use n-contacts consisting of superlattice. To understand the influence of this superlattice contact on the optical response, a study to determine the effective mesa size was carried out. As the pixels get smaller, and the quest towards higher fillfactor continues, the distance between each pixel also decreases and the risk of cross talk between pixels increases. This was our motivation for doing the study on lateral diffusion. Position-sensitive photocurrent measurements were performed and showed hole lateral diffusion length in the range of a few μm.

VLWIR detectors are used for example for space and earth observation applications. Large imaging arrays in this wavelength range need excessive cooling, and the ability to increase the cooling temperature and hence lower the system weight is valuable for these applications. A detector with 100 % cut off at 13 μm and BLIP (background limited infrared photodetector) temperature at 60 K was produced and will be discussed.

To conclude: type-II superlattice is an important future detector technology with many applications in different wavelength ranges and some of the recent IRnova results on the topic will be presented below.

2. MWIR DETECTOR

2.1 Experimental details

The MWIR detectors in this report have a homojunction p-i-n structure, which was grown on n-type (Te-doped) GaSb (100) substrate using solid source molecular beam epitaxy (MBE). The growth was performed using a VG-80 system, which was equipped with valve cracker sources for the group V (Sb_2/As_2) fluxes and SUMO® cells for the group III (Ga/In) fluxes. The superlattice consists of 10 monolayers (ML) InAs/10 ML GaSb. The active layer consists of 460 undoped SL (superlattice) periods in-between the Si-doped n-contact SL layer and the Be-doped p-contact GaSb layer. The total grown layer structure is about 3 μm thick. The doping concentration of the undoped region is $\sim 5\times10^{16}$ cm^{-3} (n-type), whereas the doping concentration of the p- and n-layers is $\sim 4\times10^{18}$ cm^{-3}.

A detector array with 320 by 256 pixels and a pixelpitch of 30 μm was produced using standard III/V-processing; mesas where formed using a combination of dry and wet etching [9], thereafter they were passivated using polymer based passivation. Mirror and contact metals were evaporated and after dicing the detector material was hybridized to an ISC9705 readout circuit chip. Eventually the substrate was fully removed. Using this process a fillfactor of 89.6 % was achieved. To study the dark currents on mesas of different sizes, single pixel detectors were also produced using the same detector design and process described above, except the substrate was not removed.

2.2 Results and discussion

An analysis of dark current mechanisms has been performed on the sample with a cut off wavelength of 5.6 μm, described above. Based on dark current measurements on mesas with different size, the dependencies for edge- and bulk currents were extracted for various biases and temperatures and the activation energy of each mechanism was analysed.
At operating temperatures above 80 K the activation energy of both edge- and bulk dark current was around 100 meV with the bulk activation energy being slightly higher. At lower temperatures (<80 K), the activation energy of both mechanisms were lower than 100 meV with the bulk mechanism activation energy being much lower than the edge currents activation energy.

The sample was encased in aluminium foil in order to reduce the photocurrent as much as possible. Still, signs of photocurrent could be seen at low bias (-100 mV) and temperature (20 K). The dark current density of two groups of mesas, one group with a side length of 30 μm and one with a side length of 90 μm is seen in **Figure 1** below. The dark current density variation between mesas with the same size is very small but there is a systematic difference in density between mesas with different sizes. The dark current density is lower for larger mesas, indicating the presence of surface currents at the mesa walls.

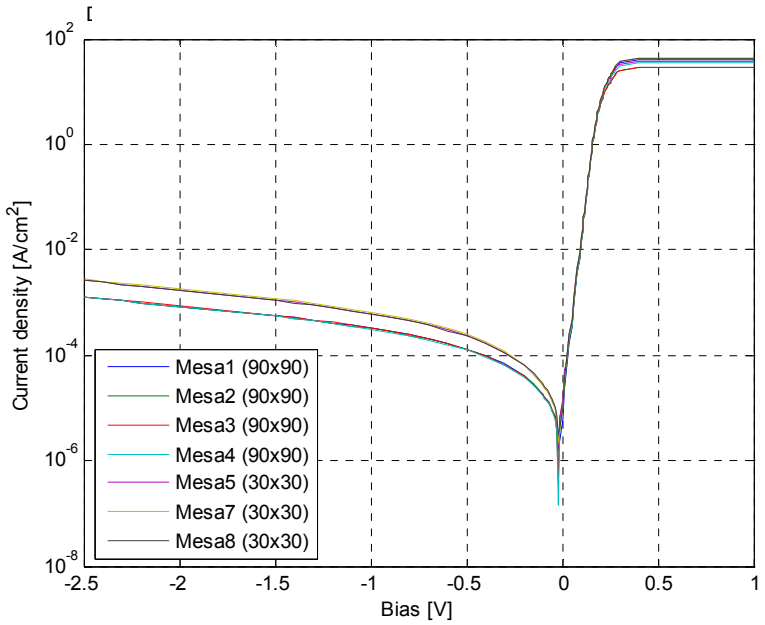

Figure 1 Dark current density of 30x30 μm^2 and 90x90 μm^2 mesas at 80 K.

The dark current at a fixed bias is extracted from measurements on one 90x90 μm^2 mesa and one 30x30 μm^2 mesa and fitted to equation 1, below:

$$Id = 4 \cdot a \cdot x + b \cdot x^2 \qquad [1]$$

Here, x denotes the mesa side length. The units of a and b are A/cm and A/cm^2, respectively, and denote surface and bulk current densities. Plots of a and b versus inverse temperature, for the different biases -50 mV, -100 mV, -500 mV and -1.0 V, were studied. The results for -50 mV are shown below in **Figure 2**.

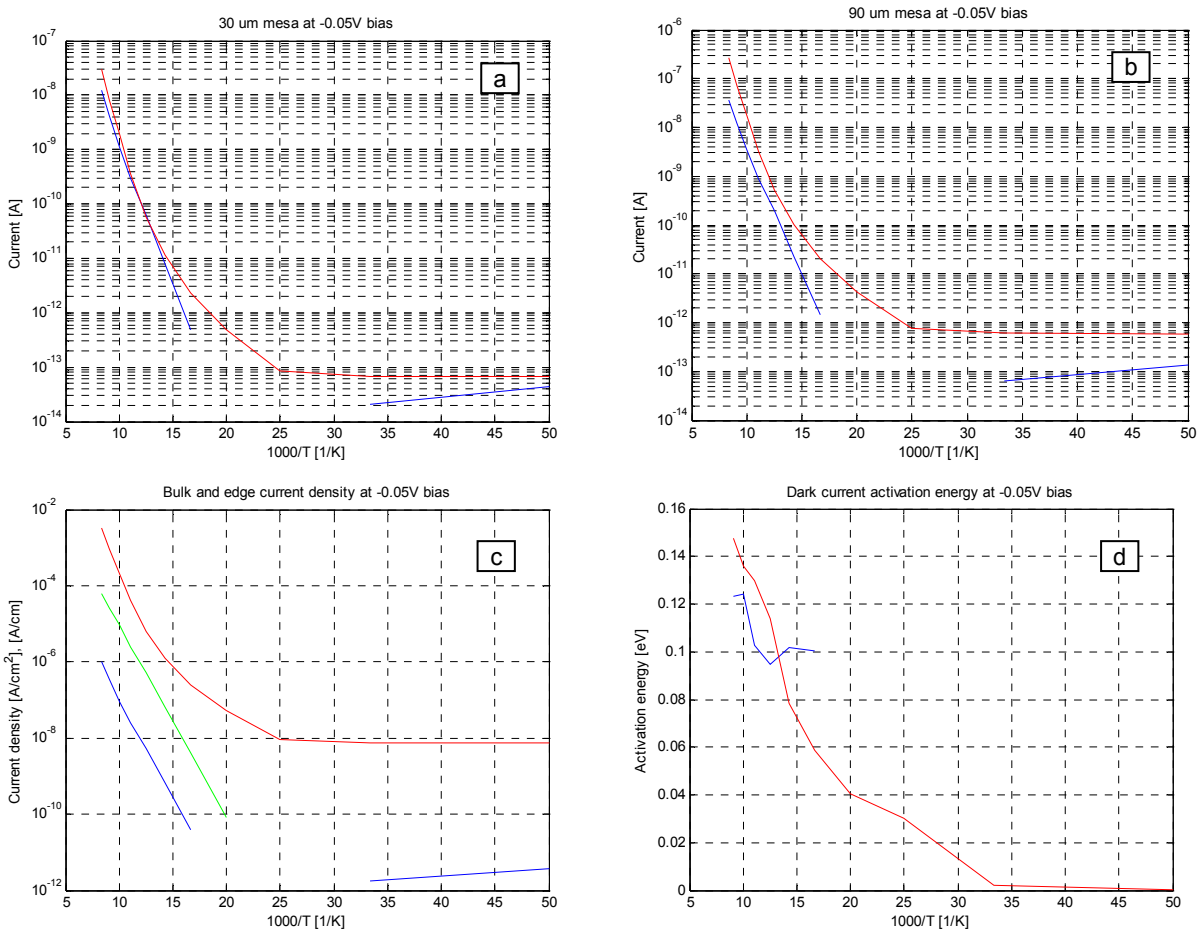

Figure 2 Extracted data from mesas at -50 mV bias.

Figure 2a and **Figure 2b** show bulk (red, solid line) and edge (blue, split line) dark current temperature dependence of 30x30 μm^2 and 90x90 μm^2 mesas, respectively. The missing edge current points have a negative value and are therefore omitted from the log-plot. This negative value is not a physical effect, but rather a measurement error as the edge current is very small at lower temperatures. For the same reason, the low temperature (20 K and 30 K) edge current values are not significant as the measurement error in this case produced positive values (with the same magnitude as the negative values) that made it into the log-plot. **Figure 2c** shows the temperature dependence of the corresponding bulk and edge current densities. The line in the middle (green) has an activation energy of 100 meV and has been added for reference. The flat section of the bulk current, below 40 K, is photocurrent that could not be avoided in the setup. At higher temperature, the activation energy of the edge current is almost constant and close to 100 meV. The activation energy of the bulk current is higher than 100 meV above 100 K but drops significantly below 70 K. **Figure 2d** shows the edge (short blue line) and bulk (longer red line) dark current activation energy as a function of inverse temperature at -50 mV bias. The value at each temperature is calculated by fitting the edge and bulk dark current component to equation 2 below:

$$Id = I_0 \cdot e^{-\frac{E_a}{kT}} \qquad [2]$$

In this equation, I_0 is the infinite temperature dark current and E_a is the activation energy, both of which are extracted from the fit.

The results for -100 mV are very similar to those at an applied bias of -50 mV. At larger negative bias, -500 mV, the activation energy of the edge current is no longer constant, but decreases with decreasing temperature. For -1.0 V, below 100 K, the activation energy of the edge dark current is significantly lower than 100 meV.

The relationship between the edge and bulk current changes little with bias with both currents having similar magnitude in 30x30 μm^2 mesas at operating temperatures around 100 K; see **Figure 2a**. The edge current is thus not insignificant in mesas fabricated with this material and process. In 30x30 μm^2 mesas it accounts for half of the dark current. In a 15x15 μm^2 mesa processed in the same way and from the same material, it would account for 2/3 of the dark current.
The activation energy of the edge current component is always smaller than the activation energy of the bulk current component at high temperature (> 70 – 80 K) while the opposite is true at low temperature. The reason for this behaviour is not clear, but one hypothesis is that surface effects, e.g. Fermi-level pinning, play a more important role at lower temperatures where thermal generation of carriers is less pronounced and bias-dependent tunnelling phenomena dominate, while a reduced bandgap at the surface leads to lower activation energy at higher temperatures where thermal generation of carriers is more pronounced.

A focal plane array was fabricated using the same detector material design but with a slightly shorter cut off wavelength, 5.3 µm. Calibrated data for spectral response and quantum efficiency (QE) from array pixels hybridized to a fan-out circuit is shown in **Figure 3** and **Figure 4** below. In this detector, the substrate is fully removed. The ripple in the curves below is due to standing waves that appeared after substrate removal. No anti-reflective coating was used.

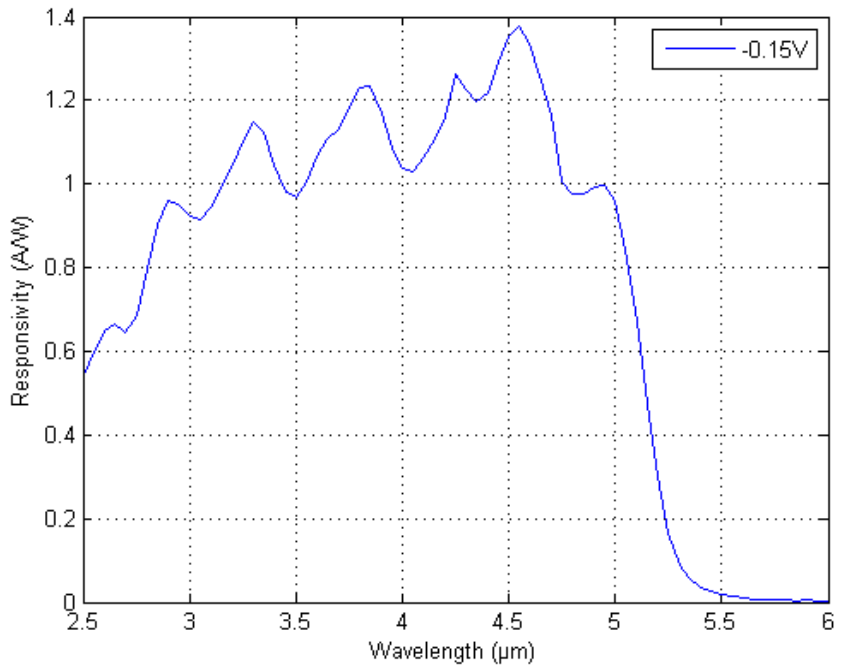

Figure 3 Optical responsivity at 120 K and -150 mV bias.

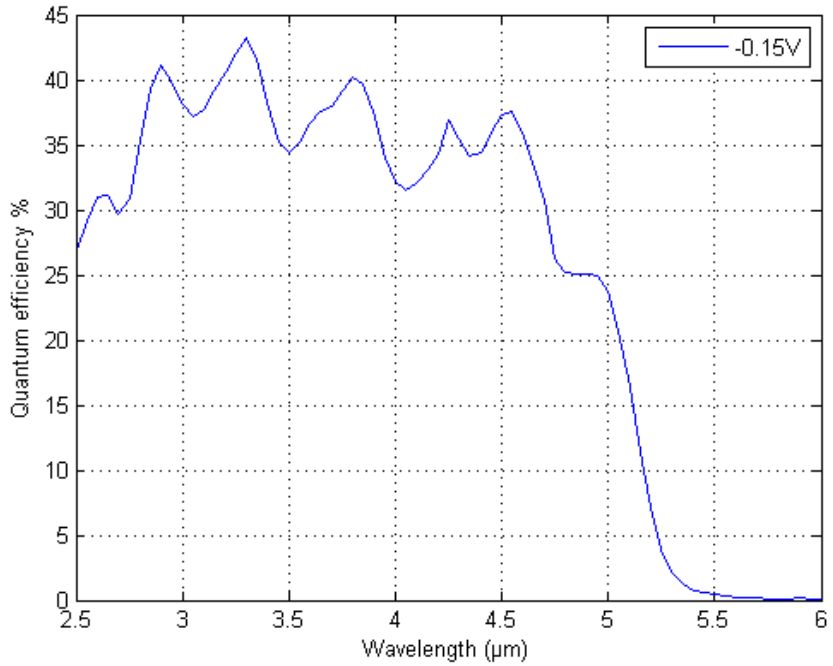

Figure 4 Quantum efficiency at 120 K.

Figure 5 below shows the dark current density from a measurement of a 7x7 array of 30x30 μm^2 mesas hybridized to a fan-out circuit. The reason that at the temperatures below 80 K the lowest current density values are at positive bias in stead of around zero is due to the incomplete thermal shielding of the sample and hence some photo current is included in the measurements.

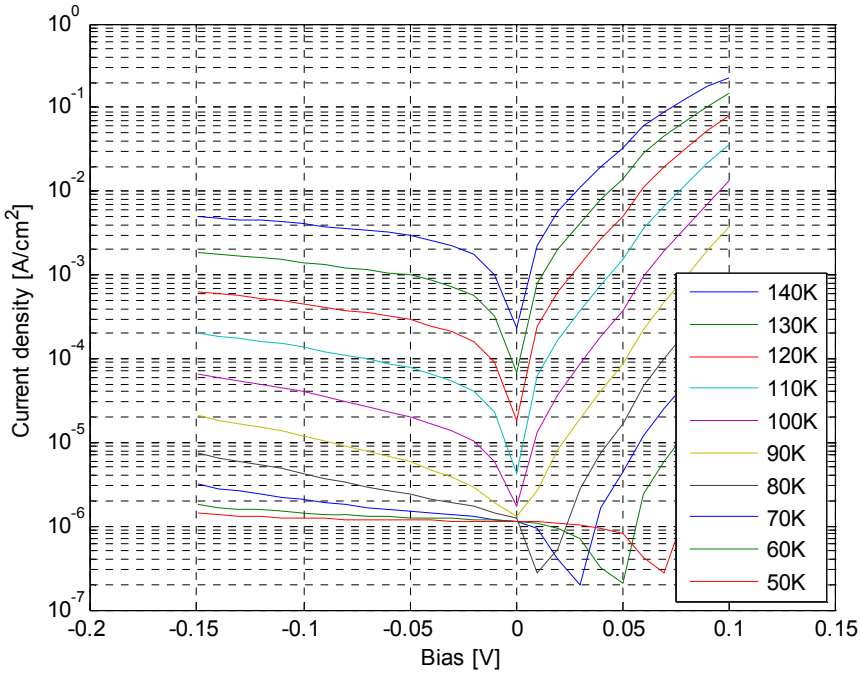

Figure 5 Dark current density at different temperatures and biases. The lowest dark current comes from the lowest temperature.

The dark current density data from the detector was analysed and fitted to a model [10]. The result can be seen in **Figure 6** below. At 60 K (**Figure 6a**) the photo current dominates close to zero bias, since the sample was not fully shielded during the measurement. At reverse bias, the trap assisted tunnelling determines the dark current.

At 100 K (**Figure 6b**), 120 K (**Figure 6c**) to 140 K (**Figure 6d**) the diffusion dark current increases faster than the generation-recombination (GR) current and becomes gradually more important. The activation energy E_a is 0.20 eV for the diffusion current, but only 0.13 eV for the GR current (presumably due to an unknown Shockley-Read center positioned halfway into the 0.24 eV bandgap).

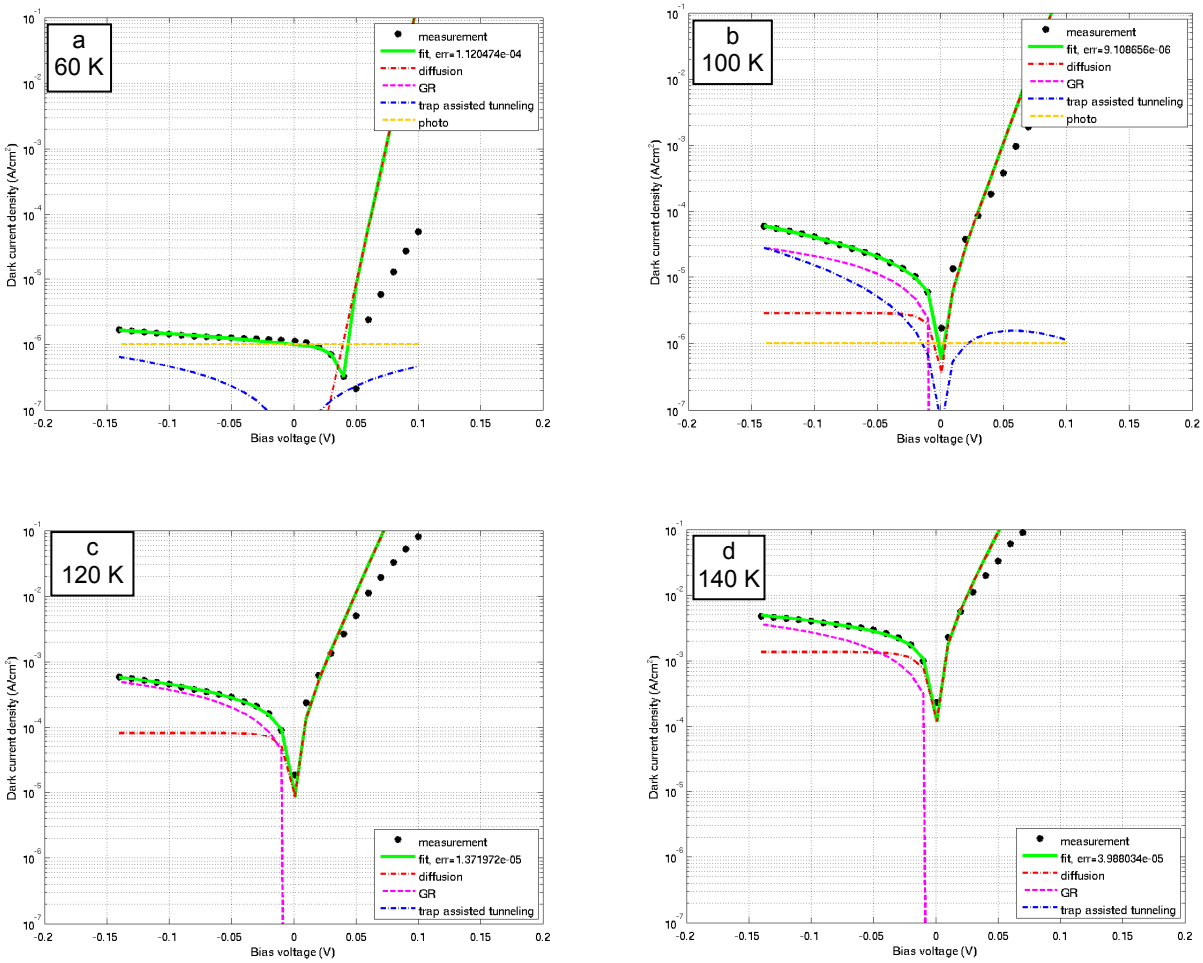

Figure 6 Measured and fitted dark current at different temperatures and biases.

After hybridization to read-out circuit ISC9705 and successful removal of the full substrate, pictures at 110 K were taken with the FPA demonstrator, see **Figure 7**. The pictures are corrected for non operating pixels and offset and gain (two point correction).

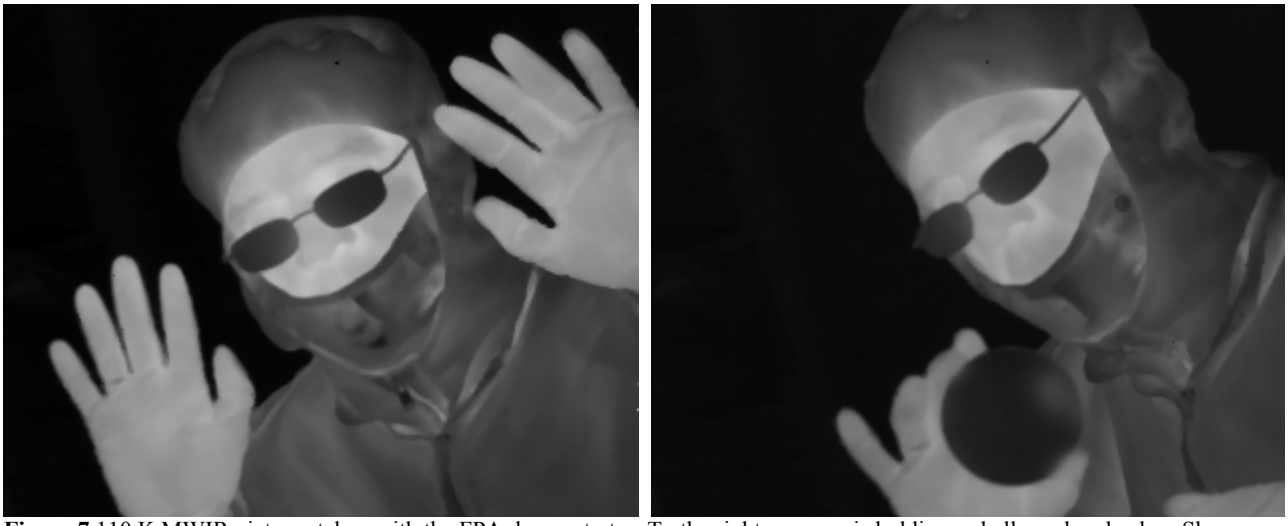

Figure 7 110 K MWIR pictures taken with the FPA demonstrator. To the right a person is holding a shallow glass beaker. She previously had her fingers where the brighter spot to the right is.

At ~100 K we measured an NETD of 34 mK using *f*/2.2 optics and 1.25 ms integration time for a well fill of approximately 20 % at 30°C. A noise floor was discovered, independent of integration time, at 2500 electrons, of which only a minor part could be accounted for by the ROIC. The rest must be attributed to noise in external electronics (AD-converter etc.). The corresponding NETD with a conventional level of electronics' noise would be 26 mK. With 50 % well fill conditions at 30°C, *i.e.* a longer integration time of 3.4 ms, this figure drops to 15 mK.

In conclusion, high-quality imaging at 110 K with a T2SL MWIR FPA has successfully been demonstrated. Despite the predicted and present dark current, these results are comparable to p-i-n detector results reported by other groups [11, 12]. This demonstrator was the first to be fabricated at IRnova. Further improvements are possible by using anti-reflection coating and by employing large bandgap material in the depletion region to reduce dark current.

3. POSITION-SENSITIVE PHOTOCURRENT MEASUREMENTS

3.1 Experimental details

To determine the effective size of the detectors, an experiment was carried out on single pixels by scanning a laser over the pixel and measuring the photo response. The bottom common n-contact is a superlattice and is expected to contribute to the photocurrent. In this experiment, the same MWIR p-i-n structure with 5.6 μm cut-off described above was used. The process to form individual pixels was essentially the same as the process used earlier to create arrays. The differences were that no passivation was used nor was the substrate removed. The measured mesa has a designed size 90x90 μm^2 with an open window of 56x56 μm^2 in the top metal contact. Due to the mesa etch process; the sample mesa sidewall has an angle of about 104°.

The sample was cooled to 77 K in an open-cycle nitrogen flow cryostat. A shield of aluminum foil, but with a small hole in order to let the laser beam pass through, was used to stop as much of the stray light as possible from reaching the device. The laser used was a 514 nm argon ion laser with a laser power of 1 mW (this power generated a reasonable photo current signal with the laser shining on the device). The laser beam generates a spot size of 2-3 μm diameter.

Different sets of IV curves were acquired across the mesa under optical pumping. The voltage was scanned from -500 mV (reverse) to +100 mV (forward). A photocurrent profile was obtained by picking out data for a constant voltage from the IV curves obtained at different locations. A coarse scan with steps of 5-10 μm steps was performed on top of the device, whereas a fine scan with steps of 1 μm was obtained close to the device edges.

3.2 Results and discussion

Figure 8 shows photocurrent generated by 1 mW laser power (1.5E4 W/cm^2), on a 88x88 µm^2 device, with -50 mV bias applied on the top p-contact. The mesa base side length is measured using SEM (Scanning Electron Microscopy) after processing. The lateral diffusion length of the holes was calculated as when the signal had fallen to 1/e of the initial value. For the measurement in **Figure 8,** the diffusion length is determined to be ~ 5 µm. The laser spot is however 2-3 µm which means the actual diffusion length would be ≤ 3 µm.

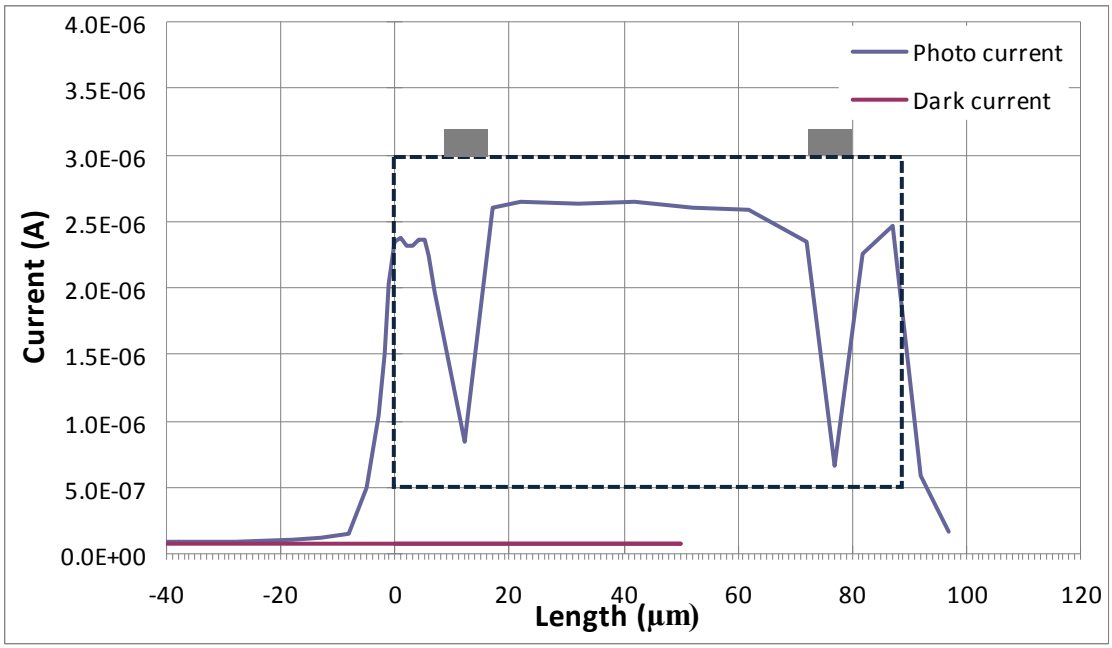

Figure 8 Photocurrent measured on sample plotted on top of a mesa cross section including contacts (squares on top). The metal contacts are blocking the laser and hence the photocurrent is lower beneath them. The flat line in the lower part of the figure is the "Dark current", *i.e.* signal when the laser is off.

The study on lateral diffusion lengths of holes is maybe not as conclusive as we would have expected, the resolution of the measurement was not high enough. However, it gives an idea of contribution from the n-contact layer outside the aimed mesa which is important as pixel density gets higher. The possibility of optical cross talk could not be dismissed.

4. VLWIR DETECTOR

4.1 Experimental details

The VLWIR detectors in this report have a barrier structure, which was grown on n-type (Te-doped) GaSb (100) substrate using solid source MBE. The superlattice consists of 12 ML InAs/5 ML $Ga_{0.75}In_{0.25}Sb$. The active layer consists of 78 undoped SL periods in-between the Si-doped n-contact (9 ML InAs/8 ML GaSb) SL layer and the p-contact layer. The total grown layer structure is about 2.4 µm thick. The doping concentration of the undoped region is $<1\times10^{16}$ cm^{-3} (n-type), whereas the doping concentration of the n-layer is $\sim1\times10^{18}$ cm^{-3}. The detector was designed for a 100 % cut off at 12 µm. Single pixel detectors were produced using wet etch mesa formation and polymer based passivation.

4.2 Results and discussion

Spectral response and external quantum efficiency (QE) of the single pixel detectors were measured; see **Figure 9** and **Figure 10**. The noise at long wavelengths (14-15 µm) is due to the fact that the light source is weak in that range. At 12 µm, the external QE is about 2 %. This measurement is made on a top lit single pixel. In a detector hybridized to a read out circuit, which is the case in an FPA, a standing wave is produced and the signal increases four times and a QE of 8 % can be reached. The absorber is only 0.4 µm thick and increasing the thickness of the absorber will increase the QE.

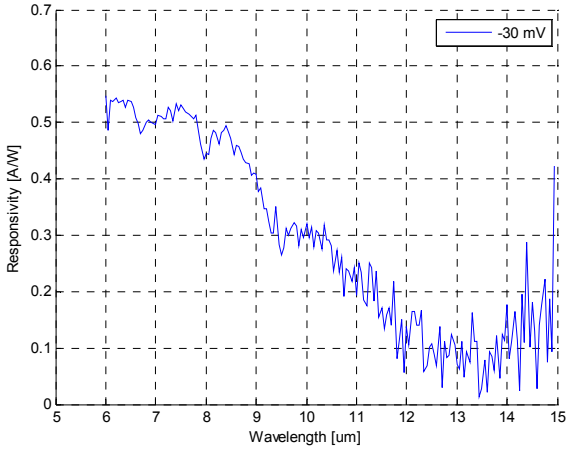

Figure 9 Optical responsivity at 60 K temperature and -30 mV.

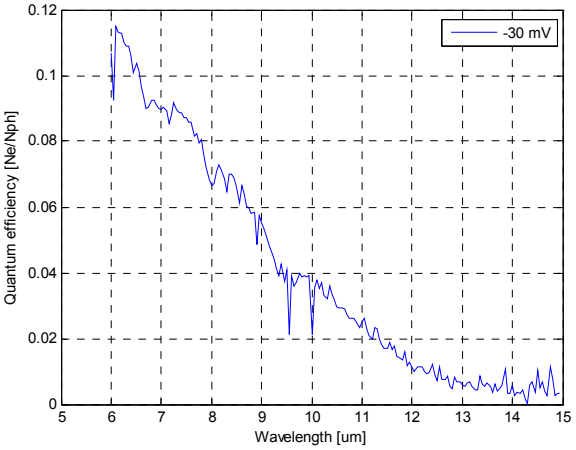

Figure 10 QE for the VLWIR structure at different wavelengths and bias -30 mV**.**

Figure 11 shows the dark current density of a 90x90 μm^2 mesa at different biases and temperatures. The dark current density at 60 K and -50 mV bias is $2x10^{-4}$ A/cm^2.

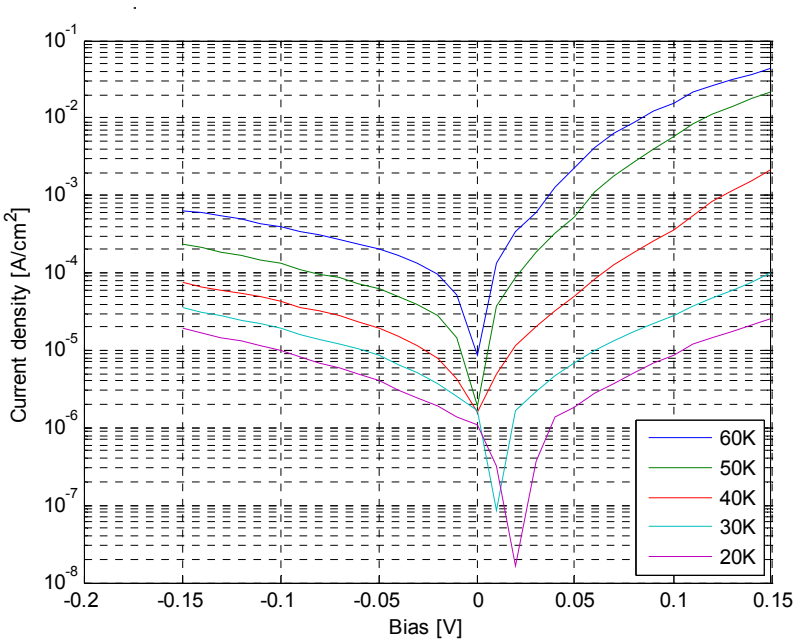

Figure 11 Dark current density at different temperatures and biases. The highest dark current comes from the highest temperature. The reason for the lowest dark current being at low positive bias is due to some photocurrent visible in this measurement. The sample was not fully shielded.

The BLIP operating temperature was calculated for half-sphere radiation from a 300 K black body. The BLIP condition was defined as the situation where the photocurrent is four times higher than the dark current. This requirement is fulfilled at 60 K (at -50 mV bias). The sample is only a single pixel and single pass radiation. For a double passage and standing wave four times higher dark current would be acceptable ($8x10^{-4}$ A/cm^2). In that case the BLIP temperature can be estimated to over 70 K for slightly negative bias. Using the limiting field of view of *f*/4 (17 times lower photo current) the BLIP temperature would be 50-60 K depending on bias.

For 60 K operating temperature and *f*/2.2 optics we estimate that the NETD would be around 20 mK and the integration time around 0.5 ms if used with ISC9705. For *f*/4 optics the NETD would increase to 40 mK, and the device would therefore require more cooling to be useful. These calculations have not taken possible mesa wall leakage currents, 1/f noise or injection efficiency into account.

In conclusion, optical responsivity in the VLWIR wavelength range from this novel detector structure has been demonstrated. Good conformance between the detector design modelling and the experimental results was achieved. Now when the concept has been proven feasible, there is room for several improvements. For example, the thickness of the absorbing layer can be increased, doping levels can be optimized and an antireflective coating can be applied.

ACKNOWLEDGEMENTS

Thanks to Vinnova – Sweden's Innovation Agency who has made this work possible through the Center of excellence IMAGIC, Sweden. Also thanks to the Swedish National Space Board who has supported the VLWIR work presented here.

REFERENCES

[1] Razeghi, M., Nguyen, B.-M., Delaunay, P.-Y., Abdollahi Pour, S., Kwei-wei Huan, E., Manukar, P., Bogdanov, S., Chen, G, "High Operating Temperature MWIR photon detectors based on Type II InAs/GaSb superlattice", Proc. of SPIE 7608, 76081Q-1-10 (2010).
[2] Smith, D. L., Mailhiot, C., "Proposal for strained layer type II superlattice infrared detectors", J. Appl. Phys. 62 (6), 2545-8 (1987).
[3] Mailhiot, C., Smith, D. L., "Long-wavelength infrared detectors based on InAs-$Ga_{1-x}In_xSb$ type-II superlattices", J. Vac. Sci. Technol. A, 7 (2), 445-449 (1989).
[4] Mohseni, H., Litvinov, V. I., Razeghi, M., "Interface-induced suppression of the Auger recombination in type-II InAs/GaSb superlattices", Physical Review B Vol. 58 (23), 15378-80 (1998).
[5] Flatté, M. E., Grein, C. H., "Theory and modeling of type-II strained-layer superlattice detectors", Proc. of SPIE 7222, 72220Q1-9 (2009).
[6] Abdollahi Pour, S., Huang, E. K., Chen, G., Haddadi, A., Nguyen, B.-M., Razeghi, M., "High operating temperature midwave infrared photodiodes and focal plane arrays based on type-II InAs/GaSb superlattices", Appl. Phys. Lett. 98 (14), 143501-1-3 (2011).
[7] Manurkar, P., Ramezani-Darvish, S., Nguyen, B.-M., Razeghi, M., Hubbs, J., "High performance long wavelength infrared mega-pixel focal plane array based on type-II superlattices", Appl. Phys. Lett., 97, 193505-1-3 (2010).
[8] Münzberg, M., Breiter, R., Cabanski, W., Lutz, H., Wendler, J., Ziegler, J., Rehm, R., Walther, M., "Multi spectral IR detection modules and applications", Proc. of SPIE 6206, 620627-1-13 (2006).
[9] Chaghi, R., Cervera, C., Aït-Kaci, H., Grech, P., Rodriguez, J. B., Christol, P., "Wet etching and chemical polishing of InAs / GaSb superlattice photodiodes", Semicond. Sci. Technol. 24, 065010 (2009).
[10] Gilmore, A. S., Bangs, J., Gerrish, A., "Current Voltage Modeling of Current Limiting Mechanisms in HgCdTe Focal Plane Array Photodetectors", J. Electron. Mat. Vol. 34 (6), 913-921 (2005).
[11] Walther, M., Rehm, R., Fleissner, J., Schmitz, J.1, Ziegler, J., Cabanski, W., Breiter, R., "InAs/GaSb type-II short-period superlattices for advanced single and dual-color focal plane arrays", Proceedings of the SPIE - The International Society for Optical Engineering Vol. 6542, 654206-1-8 (2007).
[12] Wei, Y., Hood, A., Yau, H., Gin, A., Razeghi, M., "Uncooled operation of type-II InAs/GaSb superlattice photodiodes in the midwavelength infrared range", Appl. Phys. Lett. 86 (23), 233106-1-3 (2005).